JCTC Journal of Chemical Theory and Computation

Article

pubs.acs.org/JCTC

Antimicrobial Peptide Simulations and the Influence of Force Field on the Free Energy for Pore Formation in Lipid Bilayers

W. F. Drew Bennett,*[,†] Chun Kit Hong,[‡,§] Yi Wang,*[,‡,§] and D. Peter Tieleman*[,∥]

[†]Department of Chemistry and Biochemistry, University of California, Santa Barbara, California 93106, United States

[‡]Shenzhen Research Institute, Chinese University of Hong Kong, Nanshan District, Shenzhen 518057, P. R. China

[§]Department of Physics, Chinese University of Hong Kong, Shatin, N.T., Hong Kong

[∥]Centre for Molecular Simulation and Department of Biological Sciences, University of Calgary, Calgary, Alberta T2N1N4, Canada

Supporting Information

ABSTRACT: Due to antimicrobial resistance, the development of new drugs to combat bacterial and fungal infections is an important area of research. Nature uses short, charged, and amphipathic peptides for antimicrobial defense, many of which disrupt the lipid membrane in addition to other possible targets inside the cell. Computer simulations have revealed atomistic details for the interactions of antimicrobial peptides and cell-penetrating peptides with lipid bilayers. Strong interactions between the polar interface and the charged peptides can induce bilayer deformations − including membrane rupture and peptide stabilization of a hydrophilic pore. Here, we performed microsecond-long simulations of the antimicrobial peptide CM15 in a POPC bilayer expecting to observe pore formation (based on previous molecular dynamics simulations). We show that caution is needed when interpreting results of equilibrium peptide-membrane simulations, given the length of time single trajectories can dwell in local energy minima for 100's of ns to microseconds. While we did record significant membrane perturbations from the CM15 peptide, pores were not observed. We explain this discrepancy by computing the free energy for pore formation with different force fields. Our results show a large difference in the free energy barrier (ca. 40 kJ/mol) against pore formation predicted by the different force fields that would result in orders of magnitude differences in the simulation time required to observe spontaneous pore formation. This explains why previous simulations using the Berger lipid parameters reported pores induced by charged peptides, while with CHARMM based models pores were not observed in our long time-scale simulations. We reconcile some of the differences in the distance dependent free energies by shifting the free energy profiles to account for thickness differences between force fields. The shifted curves show that all the models describe small defects in lipid bilayers in a consistent manner, suggesting a common physical basis.

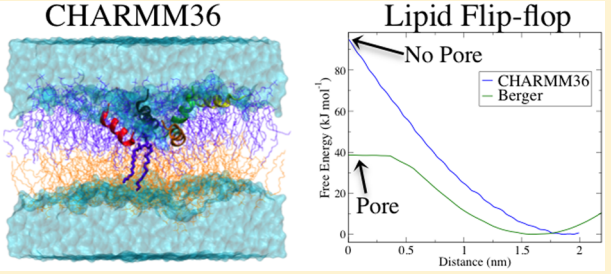

INTRODUCTION

Many antimicrobial peptides (AMPs) are short and amphipathic and have multiple charges, usually cationic amino acids.[1] It has been well established that many AMPs function through a membrane disrupting mechanism,[1] although the molecular level details are still being investigated. There are also many cell-penetrating peptides (CPPs), both natural (e.g., TAT binding domain of HIV) and synthetic (e.g., nona-arginine) that are able to translocate cellular membranes and deliver cargo molecules.[2] AMPs and CPPs have been shown to cause leakage of model membrane vesicles,[3] as have many other diverse peptides, including amyloid peptides,[4] and other molecules such as dendrimers.[5] A molecular level description for membrane pore formation is of interest in a broad range of biophysical problems.

CM15 (KWKLFKKIGAVLKVL-NH2) is a synthetic AMP made from two parent AMPs, cecropin A and melittin.[6] While cecropin A shows minimal activity against eukaryotic cells,[7] melittin is a hemolytic toxin.[8] Combining residues 1−7 of the former peptide with residues 2−9 of the latter, CM15 is a 15-amino acid (aa) AMP with a net charge of +6. It retains the potency of cecropin A without the hemolytic activity of melittin.[6] However, fluorescence leakage experiments clearly demonstrate that CM15 can disrupt vesicles made from the zwitterionic lipid POPC,[9] which is a major component of the eukaryotic membrane. Similar results have been reported for another cecropin-melittin hybrid AMP.[10]

Molecular dynamics (MD) computer simulations have been used extensively to study AMPs and CPPs.[11,12] Previous work has revealed spontaneous pore formation and peptide insertion into the lipid bilayer center.[13−15] Of note, many of the papers that reported AMP and CPP-induced pore formation used GROMOS and Berger lipid force fields.[13−16] Recently, binding free energy calculations for single AMPs have been performed, which show that the slow relaxation time for the zwitterionic

Received: March 14, 2016
Published: August 16, 2016

lipid head groups binding to the charged peptide creates a serious sampling problem.[17] Another study simulating multiple AMPs in different force fields (FFs) revealed the strong dependence of simulation results on FF parameters and suggests that multimicrosecond simulations are needed if quantitative agreement between simulation and experimental results is to be achieved.[18] In addition, the cooperative self-assembly of multiple peptides, in water, at the interface, and within the membrane core are expected to occur on an even longer time scale.

Limitations on the available computer power have inspired many studies of simpler model systems. We, and others, have studied lipid flip-flop and pore formation with atomistic computer simulations.[19−21] As a lipid headgroup moves across the hydrophobic interface a water defect forms, where water and head groups bend inward, creating a dimple in the membrane interface (often termed a water defect). Placing a single lipid headgroup at the center of a sufficiently thin lipid bilayer caused a water pore to form across the membrane. Because of the simplicity of the system we were able to determine free energies for pore formation as well as free energy decompositions in enthalpic and entropic components, showing the energetic barrier for pore formation is due primarily to unfavorable entropy.[22] These simulations are computationally challenging given the long equilibration times for lipid motions and hysteresis effects near transition states for pore formation or flip-flop. Although a general physical mechanism has emerged, accurate numerical results remain difficult to obtain and are likely to depend on details of the simulation setup and choice of reaction coordinate.[23,24]

In order to elucidate the behavior of CM15 in various membranes, we conducted over 30-μs simulations on the special-purpose machine Anton.[25] We simulated three model bilayers, namely, POPE:POPG (1:1) and POPC:cholesterol (2:1), as well as a pure POPC bilayer. Throughout the rest of the manuscript, we will refer to the first two bilayers as PE:PG and PC:CHL, respectively. Contrary to previous shorter simulations on similar peptides, we did not observe pore formation in any of our simulations. To explain this discrepancy we conducted free energy calculations on simpler, small bilayers, including thin DMPC and DLPC and thicker POPC bilayers with different force fields. The free energy for pore formation varies widely for the thinner membranes for different force fields, suggesting different lipid force fields have much different propensities for bilayers to form pores. Surprisingly, the free energy for water defect formation is very similar for all the models, by shifting the curves to account for thickness differences. To show this is a general phenomenon and not restricted to lipid flip-flop, we show that PMFs for a single arginine side chain are substantially different using different force fields; but, by correcting for membrane thickness, the free energy for arginine moving from the interface to the membrane center is virtually identical for the different models. We discuss these results and their implications on molecular dynamics computer simulations of antimicrobial peptides.

METHODS

CM15 Simulation System Preparation. Equilibrated structures of POPE:POPG (1:1), POPC, and POPC:cholesterol (2:1) were taken from our previous Anton simulations.[26] Consistent with experimental conditions, the C-terminus of CM15 is amidated.[9] A list of constructed systems is provided in Table 1. The system 1CM15-POPC-u is labeled "-u" to reflect the initially unfolded state of CM15 and distinguish it from the system 1CM15-POPC, where CM15 is in the initially folded state (Figure S1). The initial states of CM15 in the rest of the systems are given in Table 1. The system 6CM15-PE:PG-lg is labeled "-lg" to reflect its larger water box than other systems. In addition to neutralizing the system, NaCl was added to all systems at a concentration of 0.14 to 0.19 M. The salt concentration in 6CM15-PE:PG-lg was ∼0.09 M due to the addition of extra water molecules. In all single-CM15 simulations, the peptide was initially placed in water. With the exception of 6CM15-PE:PG-lg, the peptides were initially placed in the upper monolayer in multiple-CM15 simulations — the equilibrium location of CM15 from the single-peptide Anton simulations was used as a reference, and six copies of CM15 were manually inserted. To avoid steric clashes, all peptide-membrane interactions were initially turned off by converting peptide atoms to dummy atoms. Starting from residue 8, the Cα atom was converted back, with an artificially increased vdW radius (from 0.2275 to 0.455 nm). This was followed by converting back two more Cα atoms at a time, i.e., residues 7 and 9, 6 and 10, ..., 1 and 15. After each backward conversion, the system was minimized for 5000 steps and equilibrated for 100 ps. Finally, all peptide atoms were converted back to their normal atom types. The above protocol amounts to gradually pushing the lipids aside and inserting the peptide residue by residue. Nonetheless, manual adjustment was occasionally needed to completely eliminate steric clashes. Following their construction, the multiple-CM15 systems were minimized for 5000 steps and equilibrated for 10−15 ns, during which the peptide backbone and phosphorus atoms from the lower monolayer were constrained in the z-direction.

Table 1. List of Anton Simulations Performed in This Study[a]

system	t (us)	bilayer	peptide	initial	final
1CM15-PE:PG	2.0	85 POPE: 85 POPG	1 CM15	W/U	L/F
1CM15-POPC-u	1.7	170 POPC	1 CM15	W/U	W/F
1CM15-POPC	1.5	170 POPC	1 CM15	W/F	L/F
1CM15-PC:CHL	2.1	140 POPC: 70 cholesterol	1 CM15	W/F	L/F
6CM15-PE:PG-lg	3.5	85 POPE: 85 POPG	6 CM15	W/F	W+L/F
6CM15-PE:PG	9.2	85 POPE: 85 POPG	6 CM15	L/F	L/F
6CM15-POPC	8.2	170 POPC	6 CM15	L/F	L/F
6CM15-PC:CHL	3.0	140 POPC: 70 cholesterol	6 CM15	L/F	L/F

[a]The initial and final locations and the secondary structure of CM15 are labeled as following: W (water), L (lipid), U (unfolded), and F (folded).

NAMD Simulation Protocols. Prior to Anton simulations, all CM15-bilayer systems were minimized and equilibrated for at least 1 ns. All minimization and equilibration were performed with the 2.8 release of NAMD[27] using the CHARMM36 force field.[28,29] A time step of 2 fs was used, with short-range forces calculated every step and long-range electrostatics calculated every 2 steps. Bonds involving hydrogen atoms were constrained using RATTLE,[30] and water geometries were maintained using SETTLE.[31] The cutoff for short-range nonbonded interactions was set to 1.2 nm, with a switching distance of 1.0 nm. Assuming periodic boundary conditions, the

DOI: 10.1021/acs.jctc.6b00265
J. Chem. Theory Comput. 2016, 12, 4524−4533

Particle Mesh Ewald (PME) method[32] was employed for computation of long-range electrostatic forces.

Anton Simulation Protocols. All the Anton simulations were performed under semi-isotropic NPT conditions (1 atm and 303.15 K). The Berendsen thermostat and barostat[33] were employed, with default compressibility (kappa = 4.5e-5), pressure relaxation time (tau = 2.0), and temperature relaxation time (tau = 1.0). Viparr 1.5.1 was used in the preparation of the simulation systems with the CHARMM36 force field. A time step of 2 fs was used throughout all simulations, with the bonded forces updated every step, and the nonbonded short- and long-range forces updated every 1 and 3 steps, respectively. Trajectories were saved every 120 ps. All the calculations were performed using Anton software version 2.6.4.

Umbrella Sampling Protocols. GROMACS v 4 was used for most of the umbrella sampling calculations.[34] Small 64 lipid bilayers were used for the free energy calculations. For all the simulations a 2 fs time step was used, updating the neighbor list every 10 steps. Water bonds and angles were constrained with SETTLE,[31] and all other bonds were constrained with the LINCS algorithm.[35] The particle mesh Ewald method[36] was used for long-range electrostatic interactions.

The Berger lipid force field[37] parameters were chosen to match our previous work on lipid flip-flop.[19,20] Lennard-Jones interactions were truncated at 0.9 nm, as were the short-range electrostatic interactions. The V-rescale thermostat[38] was used to maintain the temperature at 323 K with a coupling constant of 0.1 ps. Berendsen semi-isotropic pressure coupling[33] was employed with a pressure of 1 bar, a compressibility of 4.5×10^{-5} bar^{-1}, and a coupling constant of 2.5 ps. For POPC and DLPC, we tested the effect of cutoff on the PMF, by simulating a bilayer with a 1.4 nm Lennard-Jones and real-space electrostatic cutoff. We also tested using the reaction field for long-range electrostatics, with a 1.4 nm cutoff for Lennard-Jones interactions and short-range electrostatics, and a reaction-field dielectric constant of 78.

We simulated the SLipids[39] with short-range electrostatic interactions cut off at 1.0 nm. A switch function was used for Lennard-Jones interactions with a 1.4 nm cutoff for the start of the switch and 1.5 nm for the potential is zero. A dispersion correction for the energy and pressure was used. The Nose-Hoover thermostat with a 0.5 ps coupling constant was used. For the barostat, the Parrinello−Rahman method was used, with a 10 ps time constant and a compressibility of 4.5×10^{-5} bar^{-1}.

For the CHARMM36 lipid parameters,[29] a switched Lennard-Jones potential was used, with a 1.0 and 1.2 nm cutoff. Real-space electrostatics were truncated at 1.2 nm. The same parameters for the thermostat and barostat used for the Berger lipids were also used for the CHARMM36 lipids. We tested the effect of the water model using TIP3p water and CHARMM TIP3p water, the latter of which has Lennard-Jones interactions on the hydrogen atoms. For CHARMM36 in NAMD we used CHARMM TIP3p water.

Unless otherwise stated, the free energy calculations were run using the GROMACS program. We did test the effect of MD engine by computing one PMF with NAMD. The umbrella sampling reaction coordinate was the distance of a single lipid headgroup from the bilayer center of mass. We restrained the single phosphorus with a force constant of 3000 kJ/mol nm^2 with 0.1 nm spacing: from 2.0 to 0.0 nm from the bilayer center. The POPC Berger curve is from our previous work,[40] but the same parameters were used as for this work. Each umbrella window was run for at least 50 ns.

The arginine side chain (propyl-guanidinium) parameters were constructed by replacing the C-α carbon with a hydrogen atom. All the parameters were the same, except the partial charges for the three hydrogen's attached to the C-β were set to be equal while maintaining arginine's +1 charge.

Our reaction coordinate is the distance to the bilayer center, meaning that for thicker bilayers the equilibrium position for the phospholipid is shifted to a larger distance along the reaction coordinate. For differences in bilayer thickness we also plot the same PMFs, but with the curves shifted along the x-axis, to account for the thickness differences.

RESULTS

Single-CM15 Simulations. We begin with single-CM15 simulations designed to estimate its equilibrium location inside a lipid bilayer. Starting with a previously equilibrated PE:PG mixture,[22] we placed a single copy of CM15 in water, approximately 2.9 nm above the phosphorus atoms of the upper leaflet. As shown in Figure S2, CM15 enters the mixed bilayer at $t \approx 138$ ns and resides in the lipid headgroup region for the remainder of the 2-μs simulation. The peptide, initially unfolded in water, folds into an α helix at $t \approx 1.06$ μs. Somewhat unexpectedly, using a similar setup, we do not observe the insertion of CM15 into a POPC bilayer: the peptide remains in water throughout a 1.7-μs simulation (1CM15-POPC-u) and folds into an α helix at $t \approx 127$ ns. We performed a second simulation (1CM15-POPC) by placing the folded CM15 closer to the POPC bilayer (0.6 nm above the phosphorus atoms of the upper leaflet). This 1.5-μs simulation reveals CM15 insertion at $t \approx 18$ ns, after which the peptide resides in the lipid headgroup region for the rest of the simulation. With this protocol, we also set up and simulated the 1CM15-PC:CHL system, where CM15 inserted into the bilayer at $t \approx 25$ ns.

The above results reflect the stochastic nature of peptide insertion as well as just how slow this process can be, relative to currently achievable simulation time scales. They also suggest that even microsecond-long simulations can be heavily influenced by initial conditions. As the dynamics of AMP insertion is not the focus of this study, no extra replicas of single-peptide simulations were performed. From the current set of simulations, we measured the average center-of-mass (c.o.m.) of CM15 inside various bilayers and analyzed the structural integrity of the membrane. These results were then used as references for simulations with multiple peptides described below.

Multiple-CM15 Simulations. By introducing multiple copies of CM15 into the simulation box, we aim to investigate the peptide-induced disruption of various membranes. Our first multiple-CM15 simulation was performed with the PE:PG mixture, where six copies of CM15 were initially added to water. The peptide:lipid ratio in this system (1:28) is comparable to that used in a previous experiment, where significant leakage of a POPC:POPG (1:1) vesicle is observed at a CM15:lipid ratio of ~1:33.[9] Nonetheless, as shown in Figure S3, only three out of the six CM15 peptides entered the PE:PG bilayer by the end of the 3.5-μs simulation. Of the three inserted peptides, two did not enter the bilayer until $t = 2.0$ μs, echoing the findings of single-CM15 simulations. We note that with three CM15 inserted, disruption of the bilayer structure appears to be rather small, e.g., the area per lipid only increased

DOI: 10.1021/acs.jctc.6b00265
J. Chem. Theory Comput. 2016, 12, 4524−4533

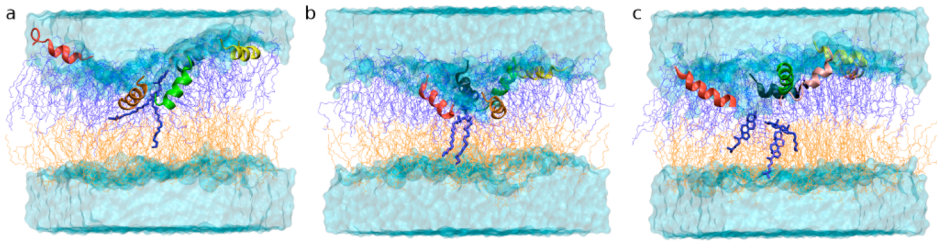

Figure 1. Anton simulation snapshots of the systems 6CM15-PE:PG (a), 6CM15-POPC (b), and 6CM15-PC:CHL (c). Water is shown in a transparent blue surface. The upper and lower lipid monolayers are colored in purple and orange, respectively. Selected lipid molecules from the upper monolayer are highlighted in thick stick representation.

marginally relative to the pure bilayer system (Figure S4), which may be explained by the somewhat symmetric locations of the three CM15, i.e., one in the upper leaflet and two in the lower leaflet.

Given that the insertion of CM15 is much slower than anticipated, in the rest of the multiple-peptide simulations, we manually placed the peptides into the upper leaflet. As detailed in the Methods section, we used the equilibrium location of CM15 in the single-peptide simulations as a reference and placed six copies of folded CM15 in the upper leaflet of PE:PG, POPC, and PC:CHL. The three systems were then simulated for 9.2, 8.2, and 3.0 μs, respectively. These simulations are designed to investigate the disruption of the bilayer structure induced by the peptides and resemble experimental conditions, where peptides only approach lipid vesicles from one side of the membrane.

Representative snapshots from the above simulations are shown in Figure 1, where selected lipids from the upper leaflet are highlighted. It is clear that all three bilayers are significantly perturbed in the presence of the six CM15, with water molecules nearly reaching the bilayer center and lipids from the upper leaflet "pushed" into the lower leaflet. The three bilayers are stretched by approximately 10% to 15% (Table 2). Although such stretching is beyond the rupture limit of membranes, lipid bilayers are known to withstand much greater tension in simulations.[15]

Table 2. Area per Lipid and P-to-P Distance of Selected Anton Simulation Systems[a]

system	A (nm^2)	A/A_0	PtoP (nm)	PtoP/PtoP$_0$
6CM15-PE:PG	0.639	1.11	3.91	0.95
6CM15-POPC	0.709	1.10	3.72	0.97
6CM15-PC:CHL	0.531	1.15	4.15	0.92

[a] A_0 and PtoP$_0$ are mean area per lipid and P-to-P distance of the corresponding pure lipid bilayer systems (PE:PG, POPC, and PC:CHL).

It is well established[12] that AMP-induced disruption of bilayer structures may take the form of pore formation in the membrane, where the amphiphilic peptides line the wall of water-filled pores and stabilize the lipid−water interface. An example is the AMP magainin, which induced spontaneous pore formation in a DPPC bilayer during 250 ns simulations.[15] In the three multiple-CM15 simulations descried above, we found that the peptides can adopt orientations nearly parallel to the membrane normal (Figure 3). However, these peptides only reside in the upper leaflet, rather than spanning the entire bilayer. While such organization perturbs the bilayer considerably, no pore formation is observed.

The perturbed bilayer structure is also evident from changes in the number density profiles and water permeability shown in Figure 2. According to these profiles, structural changes appear to be the largest for PC:CHL, where the hydroxyl group of cholesterol is frequently found near the bilayer center (also see Figure 1c). In contrast, CM15-induced structural changes are much smaller in the POPC bilayer, which also shows minimal increase in water permeability compared with its pure lipid counterpart (Figure 2d). Despite the increased water permeability, no continuous water file is observed in any of the above simulations. The deep penetration of water molecules shown in Figure 1, which reflects local defects in a bilayer, is quickly "fixed" within a few nanoseconds. Furthermore, although lipids from the upper leaflet are frequently "pushed" into the lower leaflet, no flip-flop of lipids is recorded. Overall, the bilayers appear to always recover from local defects throughout our microsecond-long simulations.

DMPC PMFs. To explain the qualitative observations from our ANTON runs and previous MD simulations, we performed umbrella sampling calculations to determine the free energy barrier against pore formation in membranes modeled with a series of force fields and/or MD programs. Previously, we have shown that moving a single lipid from water to the center of the lipid membrane caused pore formation.[19] Figure 4 shows the free energy for moving a single DMPC phosphate group from its equilibrium position to the center of the bilayer. Our reaction coordinate for the umbrella sampling calculations is the distance from the center of mass of the phosphorus atoms to the center of mass of the bilayer but only in the direction normal to the plane of the bilayer. For different lipid force fields, a free energy trough is revealed at the equilibrium position of the phosphate groups in the bilayer. Moving the phosphate into the bilayer core causes an increase in the free energy. Clearly, the biggest outlier is the Berger lipid parameters, with a barrier for lipid flip-flop roughly half as large as the other models predict. At ∼0.4 nm from the bilayer center the free energy plateaus at 39 kJ/mol, while it continues to rise to around 80 kJ/mol and above for CHARMM36 lipids and the Slipids.

The steep slope in the PMF as the lipid moves into the bilayer core corresponds to the formation of a water defect − the interface bends inward to maintain interactions with the flipping lipid. For the Berger lipids, when we restrained the phosphate of a single lipid at 0.5 nm a water defect is observed (Figure 5), while when the phosphate is placed within ∼0.4 nm of the bilayer center a pore in the membrane opens, which causes the free energy to plateau. The pore is hydrophilic with water and lipid head groups forming a disordered toroidal shape in the membrane (Figure 5). For the CHARMM36 force field a pore is never observed, and the PMF has a peak at the

DOI: 10.1021/acs.jctc.6b00265
J. Chem. Theory Comput. 2016, 12, 4524−4533

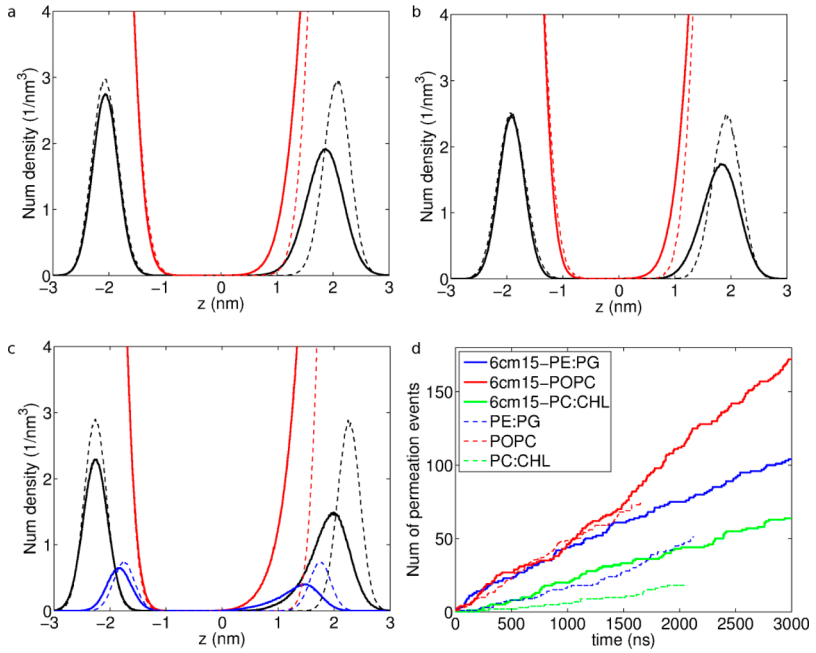

Figure 2. Changes in bilayer structure and water permeability upon the insertion of six CM15. (a-c) Number density profiles of phosphorus atoms (black) and water oxygen atoms (red) in systems 6CM15-PE:PG (a), 6CM15-POPC (b), and 6CM15-PC:CHL (c). The number density profiles of the corresponding pure lipid systems (PE:PG, POPC, or PC:CHL) are shown as dashed curves. The blue curves in (c) are number density profiles of the hydroxyl oxygen in cholesterol. Throughout the calculation, the lower leaflet of the CM15-bilayer systems is aligned with that of the pure lipid systems. (d) Number of water permeation events in 6CM15-PE:PG, 6CM15-POPC, and 6CM15-PC:CHL, as well as the corresponding pure lipid systems. For clarity, only the first 3-μs data is shown for 6CM15- PE:PG and 6CM15-POPC. To improve statistics, the trajectory of 1CM15-POPC-u is also used in the calculation of water permeation events through a pure POPC bilayer. The calculation of permeation events follows our previous study.[26]

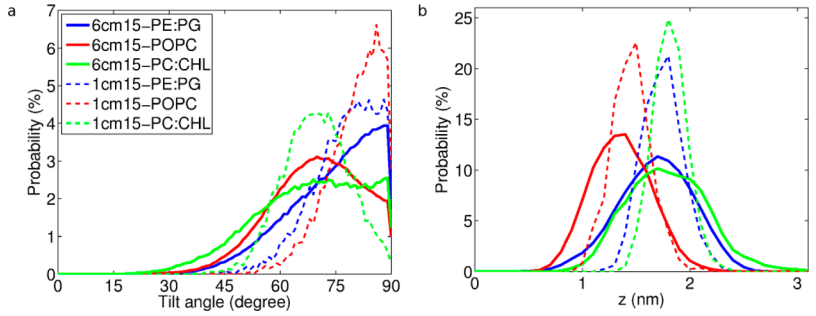

Figure 3. Histograms of CM15 tilt angles (a) and c.o.m. (b) in Anton simulations. Peptide tilt angle is defined as the angle between the z-axis and a line connecting the Cα atoms of residue 5 and 12 of CM15. Histograms of tilt angles and c.o.m. are obtained with a resolution of 1 degree and 0.1 nm, respectively.

bilayer center. The Slipids are similar to the CHARMM36 results, except for right at the bilayer center, where we observe a transition between the water defect and pore states (Figure 6). For the Slipids the defect is observed to flip from one leaflet to the other during the 100 ns simulation with a phosphate restrained at the bilayer center.

Shifting the PMFs along the x-axis to account for the thickness differences between the models shows that the free energy for defect formation is similar for all force fields. The bottom panel of Figure 4 shows that the shifted PMFs are the same for Berger, Slipids, and CHARMM36 lipids from 2.0 nm to ~0.7 nm and very similar for the Slipids and CHARMM36, although CHARMM36 extends further because it is the thickest membrane. Now the main differences between the models are that the Berger DMPC bilayer forms a pore, and the PMF plateaus and the CHARMM36 DMPC bilayers (in GROMACS without CHARMM TIP3p water which has Lennard-Jones interactions on the hydrogen atoms) are thicker than the other models.

POPC PMFs. From Figure 5, for DMPC we showed that by accounting for thickness differences, the models are very similar, except when there is a transition to a pore state. Therefore, in thicker bilayers where none of the models predict a pore state for lipid flip-flop we should expect very similar PMFs. Figure 7 shows the PMFs for moving a single POPC headgroup into the center of a POPC bilayer for the Berger and CHARMM36 force fields. The free energy peak is higher for the CHARMM36 bilayer (~100 kJ/mol) compared to the Berger force field (80 kJ/mol). We do not observe pore formation in either of the models - with only a water defect formed when the lipid is right at the center of the bilayer. The bottom panel shows the PMFs, with the Berger curve shifted by an arbitrary distance along the x-axis to align it by eye with the CHARMM36 curve. We tested the effect of run parameters on

DOI: 10.1021/acs.jctc.6b00265
J. Chem. Theory Comput. 2016, 12, 4524−4533

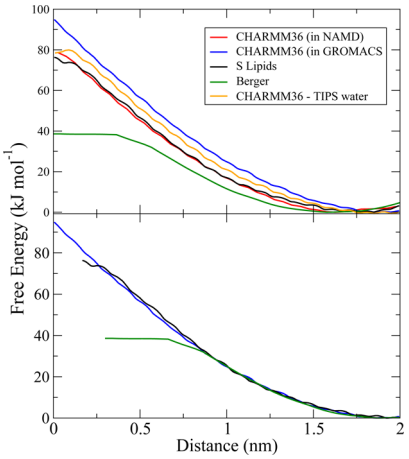

Figure 4. DMPC PMFs using different force fields with GROMACS and NAMD. For CHARMM36 lipids in GROMACS, we used both regular TIP3p water (blue) and CHARMM TIP3P water (orange). For the umbrella sampling calculations, we restrain the phosphorus of a single lipid at a varying distance from the bilayer center of mass, in the direction normal to the plane of the bilayer. In the bottom panel, we shifted the curves along the *x*-axis to account for the difference in bilayer thickness for each force field compared to CHARMM36 (in GROMACS) (blue curve).

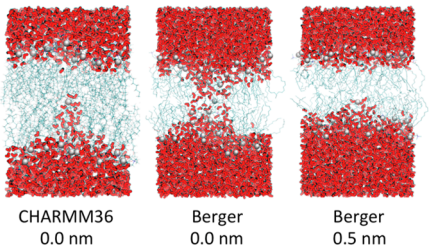

Figure 5. Structures of the DMPC bilayer with a lipid headgroup in their interior with different force fields. Water molecules are red, lipid tails are cyan, and lipid phosphorus atoms are gray balls. With the CHARMM36 force field water is pulled into the center, forming a single leaflet water defect. A large pore forms for the Berger force field with a lipid headgroup at the bilayer center, while a water defect forms at 0.5 nm from the bilayer center.

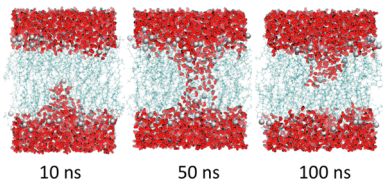

Figure 6. Snapshots for the DMPC bilayer using the Slipids force field simulation with a lipid headgroup restrained at the bilayer center. Colors are the same as in Figure 5. We observed a spontaneous transition from a defect on one leaflet, an intermediate pore, and then a defect on the opposite leaflet.

the POPC PMF for the Berger model by increasing the Lennard-Jones and real-space electrostatic interaction cutoff to 1.4 nm. This caused the lipid tails to attract more and increased the bilayer thickness, deceasing the area per lipid, in better agreement with CHARMM36. The PMF is very similar to CHARMM36, although we do observe a slight trough right at the bilayer center, because the water defect flipped to the opposite leaflet part way through the simulation. The reaction-field method for long-range electrostatics was used for a PMF

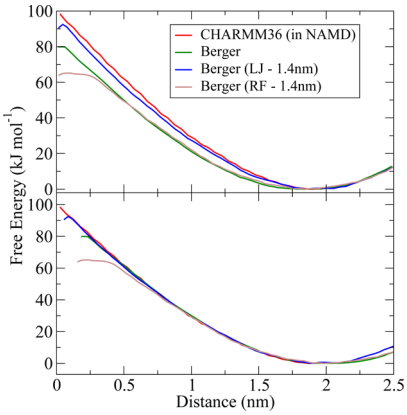

Figure 7. POPC PMFs for the Berger and CHARMM36 force fields. The coloring scheme is the same as Figure 4. The Berger (LJ − 1.4 nm) curve was run with the exact same setup as the Berger curve, but with an increased cutoff of 1.4 nm, compared to 0.9 nm.

with Berger lipids. Despite using the longer cutoff for Lennard-Jones interactions, the PMF with reaction-field is very similar to the Berger PMF with a 0.9 nm cutoff. Although near the center of the bilayer, the reaction-field PMF flattens, due to a pore forming, reducing the free energy for lipid flip-flop.

To explore the extent of the discrepancy between the models we further investigated lipid flip-flop in short DLPC lipid bilayers. Previously, we showed that the barrier for pore formation in a DLPC bilayer was sufficiently low that we could observe spontaneous pore formation in equilibrium simulations, matching (within statistical error) the probability calculated from umbrella sampling.[20] For the Slipids there is a ∼50 kJ/mol barrier and ∼65 kJ/mol for CHARMM36. These numbers would suggest that the bilayer is relatively stable, with very infrequent pore formation. We also tested the effect of increasing the Lennard-Jones and real-space electrostatic interaction cutoff to 1.4 nm, which increased the DLPC bilayer thickness. The Berger DLPC PMF with the longer cutoff is very similar to the Slipid PMF, with the same free energy barrier, although the initial steep slope is in between the Slipid and CHARMM36 curves. The PMF for DLPC with the reaction-field method for long-range electrostatic interactions has a similar slope as the Slipid model but has a barrier for flip-flop roughly half way between the Slipid and Berger models with 0.9 nm cutoffs and PME. Shifting the curves along the *x*-axis gives relatively good fits for the water defect free energy given the noise in the PMFs. The Berger PMF with the reaction field method slope does not match as well as the other models.

Arginine Side Chain PMFs. We show that water defect formation is a general mechanism, not limited to lipid flip-flop, by computing PMFs for a single arginine side chain moving from water to the center of a DMPC bilayer. Figure 8 shows the free energy profiles for arginine using the Slipids and AMBER99 arginine parameters and CHARMM36 lipids with CHARMM27 arginine and regular TIP3p water. There is a significantly deeper free energy minimum for the CHARMM PMF, as well as a larger maximum at the bilayer center. These results match previous simulations of arginine and lysine PMFs using different force fields.[41] At the bilayer center a single sided water defect is formed for each bilayer, with no pores observed. If we shift both curves along the *x*-axis to account for the DMPC bilayer thickness differences and the *y*-axis so that the free energy is zero at their free energy minima, the free energy

DOI: 10.1021/acs.jctc.6b00265
J. Chem. Theory Comput. 2016, 12, 4524−4533

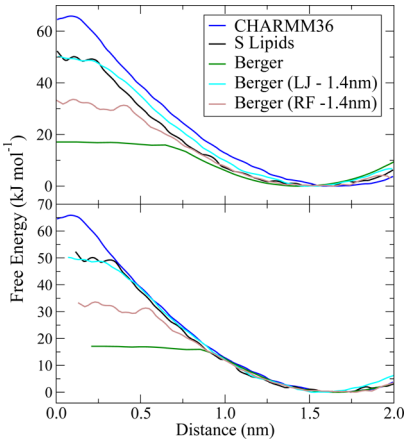

Figure 8. PMFs for moving a single DLPC lipid into the center of a DLPC bilayer. The method, coloring scheme, and bottom panel are described in Figure 7.

curves for arginine insertion for the two models are very similar. Now the difference between the models is the free energy for arginine moving from water to the lipid interface, with a difference of ∼7 kJ/mol. This suggests that the two models have similar energetics for arginine entering the hydrophobic membrane core, which is related to the formation of a water defect in the lipid bilayer.

DISCUSSION

Despite the diversity in their sequences and structures, AMPs achieve their antimicrobial effect primarily through permeabilizing cellular membranes.[12,42] The permeation pathway created by AMPs is often characterized by either a barrel-stave model, a toroidal pore model, or a carpet mechanism, depending on the structure of the pathway and the form of peptide-lipid interactions. The first two models both involve a well-defined pore, the wall of which is either lined by AMPs alone (barrel-stave model) or by both AMPs and lipid headgroups (toroidal pore model). The carpet mechanism can be viewed as an extreme form of the toroidal pore model, where the membrane undergoes detergent-like disintegration.[12] Computer simulations have been used extensively to study AMPs, as well as many other membrane poration applications. Recent progress in lipid force field parameters will drive a renewed interest in these studies. How does the choice of force field affect the expected result, for example in simulations of AMP induced membrane poration?

While the exact mechanism by which CM15 permeabilizes a membrane remains to be fully elucidated, its parent peptide, melittin, has been shown to form toroidal pores.[43,44] Previous experiments have demonstrated that similar to melittin, CM15 can induce significant leakage in both PE:PG and POPC vesicles.[9] With our 30-μs MD simulations, we investigated the disruption of CM15 on three model bilayers, including a PE:PG (1:1) mixture and a pure POPC bilayer, as well as a PC:CHL (2:1) mixture. The peptide:lipid ratio in our simulations (6:170) is comparable with those used in experiments.[9] Nonetheless, while CM15 is found to cause considerable perturbation to the membranes, it did not permeabilize any of the three bilayers. Overall, the impact of CM15 appears to be highly restricted to the upper monolayers, where the peptides are inserted. Perturbation to the lower monolayers is minimal, as can been seen from their largely unaffected number density profiles (Figure 2). Throughout the microsecond-long simulations, we did not observe the formation of a continuous water file, which is assumed to be the prerequisite for the leakage of fluorescent dye molecules.

The above simulation results are in contrast to previous studies performed on AMPs comparable in size and net charges to CM15. For instance, simulations[14,15,45] have been performed to study magainin (23 aa, + 3 net charges) and melittin (26 aa, + 6 net charges) as well as the cyclic BPC194 (10 aa, + 6 net charges) based on the Berger and GROMOS or their compatible force fields.[46−48] These peptides are shown to spontaneously form disordered toroidal pores in DPPC or DPPG bilayers within tens to hundreds of nanoseconds. The pore formation process involves a key intermediate state, where the deeply inserted AMPs establish interactions with solvent molecules and lipid head groups from the peptide-free monolayer. Once this intermediate state is reached, pore formation often ensues, creating a permeation pathway for both water and lipids, i.e., lipid flip-flop is readily achieved through the toroidal pores. HIV-1 TAT, a cell-penetrating peptide, has also been shown to induce pore formation using the Berger lipids and GROMOS peptides,[13,16] where the transient pores are used by the peptide to translocate across the membrane.

Our Anton simulations used similar system sizes and peptide:lipid ratios as in these previous studies. Nonetheless, a clear difference between our simulations and previous studies is the absence of the intermediate state described above. While we cannot rule out the possibility that our simulations are kinetically trapped, i.e., CM15 may permeabilize the membranes in longer simulations, the time scale of the Anton runs, the largely localized membrane defect, and the lack of an intermediate state hint at an artificially enhanced stability of the bilayers in our simulations. We note that a recent study on arginine-rich cell-penetrating peptides suggested a kinetic model for their membrane translocation, although it is unclear whether CM15 is capable of adopting this model.[49] A recent Anton simulation of the AMP PGLa using the CHARMM force field also did not reveal any pore formation over one microsecond of simulation.[18]

One major difference between our CM15 simulations and previous simulations observing AMP induced pore formation is the force fields used. Our free energies of pore formation show that the energetic barrier depends strongly on the force field and parameters. Using different atomistic force fields we find different free energies for lipid flip-flop in DLPC, DMPC, and POPC lipid bilayers. The relatively old Berger lipid parameters predict a much lower free energy barrier for lipid flip-flop in DLPC and DMPC, due to the formation of a hydrophilic pore across the lipid bilayer. More recent CHARMM36 and Slipids force fields predict a much greater barrier for lipid flip-flop (by over 40 kJ/mol) in the DMPC bilayer compared to the Berger lipid parameters. Increasing the Lennard-Jones cutoff caused the Berger bilayers to become thicker and made the free energy profiles very similar to Slipid and CHARMM36. Using reaction-field for long-range electrostatic calculations reduced the free energy barrier for pore formation. The larger energy barrier for lipid flip-flop is consistent with our observation that microsecond-long simulations of the antimicrobial peptide CM15 in a POPC bilayer with the CHARMM36 force field did not induce pore formation. Earlier simulations with the Berger lipid parameters, and often with reaction-field electrostatics, observed pores with antimicrobial peptides because the free energy for pore formation with Berger parameters would result

DOI: 10.1021/acs.jctc.6b00265
J. Chem. Theory Comput. 2016, 12, 4524−4533

in orders of magnitude more frequent pore formation compared to CHARMM and Slipids. We are not directly equating the two processes, as the peptide binding to the interface would be another major energetic component and perturb the interfacial properties of the membrane in force field dependent ways. Indeed, a corollary of this work is the difference in interfacial binding energy for arginine for the CHARMM force field compared to AMBER (see Figure 9). Nonetheless, the 40 kJ/mol difference in free energy described above suggests that pore formation is strongly force field dependent.

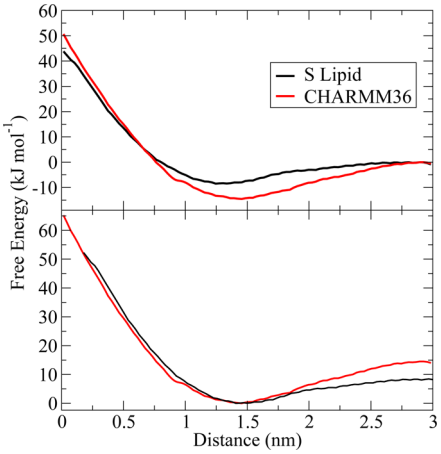

Figure 9. PMFs for transferring a single arginine side chain across a DMPC bilayer with the Slipids and the CHARMM36 lipids. In the bottom panel we shifted both curves to have their minima at 0 kJ/mol and the Slipids curve by the difference in thickness between CHARMM36 and Slipids bilayers (Table 2).

As the lipid crosses the bilayer there is a transition from a flat bilayer to water defect—a hydrated dimple forms to maintain the lipid's interactions with water and other lipid head groups. This corresponds to a steep increase in free energy. For some lipids, as the lipid moves closer to the bilayer center, at a certain point a pore forms. At this point the free energy profile plateaus because there is equal force on the lipid toward either leaflet within the pore. For the Berger lipids there is a clear transition point for DMPC and DLPC but not for the thicker POPC bilayer. All the models predict the same trend that DLPC < DMPC < POPC for the free energy of moving a lipid into the bilayer center, as expected from the thickness of the bilayers and previous simulations.[21,50] Accurately modeling these collective phase transitions is a challenge for atomistic MD simulations, due to slow lipid diffusion and collective dynamics, periodic boundary conditions, and finite simulation sizes. It should be noted that our one-dimensional reaction coordinate has a hysteresis between the defect state − pore state − and the water defect on the opposite leaflet. A more elaborate reaction coordinate for arginine partitioning showed that the barrier height is slightly lower than predicted with a 1D reaction coordinate.[51] Another study using local densities as the reaction coordinate found a larger free energy barrier for DPPC flip-flop[24] than that predicted by our previous 1D PMF.[19] This can be explained by our present results, as they used CHARMM36 lipids, and our results were with Berger parameters. More recently, Awasthi and Hub computed pore formation PMFs using three different reaction coordinates, which were all found to suffer from strong hysteresis. The authors suggested that the transition state of pore formation was characterized by the formation/disruption of a membrane-spanning water channel, which would serve as a better reaction coordinate.[23] Other systematic studies of pore formation using, for example, electroporation, ion gradients, or mechanical stress in membranes are of interest and might help link the simulations to experimental results.

By accounting for lipid bilayer thickness we show that each of the models have similar curves for the initial insertion of a lipid headgroup or arginine into the hydrophobic core of the lipid bilayer, which is accompanied by the formation of single sided water defects. This result is encouraging, given the importance of small defects in membranes when simulating transmembrane proteins and peptides, drugs, and many other polar solutes. Explaining the energetic reason for the similarity is not straightforward but may point to a basic underlying physical basis for this process. Previously we showed that water defect was enthalpically unfavorable, while pore formation was entropically unfavorable.[22] Therefore, each model gets the enthalpic defect formation correct, but the transition to a pore is more difficult to accurately model because it involves a large change in the degrees of freedom in the system. By using a longer cutoff for Lennard-Jones and real-space electrostatic interactions the free energy for POPC and DLPC lipid flip-flop is increased for the Berger lipids. Previous simulations have also shown this effect for DPPC flip-flop with Berger lipids.[52] Running simulations with reaction-field for long-range electrostatics reduces the free energy for pore formation. Using different TIP3p water models with CHARMM36, we show that the agreement with NAMD is better using the proper CHARMM TIP3p model that has hydrogen Lennard-Jones interactions; but, by accounting for thickness differences, we show that the water model or run parameters do not affect the free energy profile for water defect formation. These results support the idea that the free energy for initial water defect formation does not depend strongly on the force field (after correcting for thickness changes) and can also be modulated by changing the run parameters. The one exception may be the use of a reaction field, where the slope as the defect gets bigger and is slightly different than the other PMFs (Figures 7 and 8). More detailed simulations and reaction coordinates will be needed to verify if this is real or noise in the profiles. We also note that the PC lipid PMFs have a similar slope, but the arginine PMF is slightly more steep (Figure S5). This suggests that different solutes will have different energetic costs for deforming a membrane. More detailed analysis and simulations will be needed to understand the source of the differences.

The large difference in free energy for pore formation with the Berger lipids compared to the CHARMM and Slipids lipids and large effect of run parameters means that the propensity of a bilayer to form pores can be tuned in simulations; but at this point it is not possible in our view to decide which model (or parameters) is closer to real systems, as the experiments also have very different estimates for pore formation and lipid flip-flop. Conventional wisdom in textbooks and reviews is that PC lipids flip-flop on the hours time scale.[53] However, there are a number of recent estimates that suggest much faster flip-flop.[54] It is not straightforward to compare our microscopic free energies with rates from experiments and will require a more thorough and multidisciplinary characterization. It seems likely that CHARMM36 and Slipids overstabilize the bilayer state, because DLPC is known to form leaky vesicles. A known problem with CHARMM27 lipids was that they formed a gel

DOI: 10.1021/acs.jctc.6b00265
J. Chem. Theory Comput. 2016, 12, 4524−4533

state in a constant pressure simulation. CHARMM36 lipids fixed this issue, but perhaps the model is still too cohesive. By increasing the cutoff for POPC and DLPC the Berger PMFs for flip-flop were similar to the CHARMM36 and Slipid results. This supports the view that lipid tail cohesion, membrane thickness, and area of the interface with water are important determinants for the free energy barrier for defect formation. A recent study comparing many force fields to NMR order parameters showed that CHARMM36 is the most reliable model.[55] Given that lipid models are designed to reproduce bilayer structural parameters it is perhaps not surprising that the energetics for a bilayer with a pore is hard to capture accurately. There are a large number of important biological processes that involve membrane pores, so reconciling the different models and experimental studies will be an important direction for future work.

CONCLUSIONS

Long time scale atomistic simulations of an antimicrobial peptide with a lipid bilayer show the peptide does perturb the bilayer interface. These simulations show how slow lipid-peptide interactions are sampled and suggest that long time scales are needed for membrane systems. No pores were observed in microsecond-long simulations, contrary to expectations from previous simulations. Extensive free energy calculations were used to explain this discrepancy and highlight large differences between popular atomistic lipid force fields. The older, united atom Berger lipids can form pores much more readily than the recent atomistic CHARMM36 and Slipids. The free energy barrier is strongly modulated by run parameters, including the Lennard-Jones cutoff and calculation method of long-range electrostatic interactions. Despite differences in the free energy barrier for pore formation, for one-sided water defects, all the models predicted very similar free energies. The large difference in free energy cost for pore formation without peptides suggests that orders of magnitude longer time scales would be needed to observe pore formation in simulations with CHARMM and Slipids compared to Berger lipids. Caution is needed when interpreting and comparing simulations of pore formation with different force fields.

ASSOCIATED CONTENT

Supporting Information

The Supporting Information is available free of charge on the ACS Publications website at DOI: 10.1021/acs.jctc.6b00265.

Figures S1−S5 (PDF)

AUTHOR INFORMATION

Corresponding Authors

*E-mail: wfdbennett@gmail.com (D.B.).
*E-mail: yiwang@phy.cuhk.edu.hk (Y.W.).
*E-mail: tieleman@ucalgary.ca (D.P.T).

Notes

The authors declare no competing financial interest.

ACKNOWLEDGMENTS

This work was supported by the Natural Sciences and Engineering Research Council (NSERC). D.P.T. is an Alberta Innovates Health Solutions Scientist and Alberta Innovates Technology Futures Strategic Chair in (Bio)Molecular Simulation. Y.W. acknowledges Project 21403183 supported by The National Natural Science Foundation of China. Y.W. also thanks Dr. J. Andrew McCammon and Dr. Judy E. Kim for their support. Anton computer time was provided by the National Center for Multiscale Modeling of Biological Systems (MMBioS) through grant P41GM103712-S1 from the National Institutes of Health and the Pittsburgh Supercomputing Center (PSC). The Anton machine at PSC was generously made available by D.E. Shaw Research. Calculations were carried out in part on Compute Canada facilities.

REFERENCES

(1) Nguyen, L. T.; Haney, E. F.; Vogel, H. J. The Expanding Scope of Antimicrobial Peptide Structures and Their Modes of Action. *Trends Biotechnol.* **2011**, *29*, 464−472.
(2) Zorko, M.; Langel, U. Cell-Penetrating Peptides: Mechanism and Kinetics of Cargo Delivery. *Adv. Drug Delivery Rev.* **2005**, *57*, 529−545.
(3) Wimley, W. C.; Hristova, K. Antimicrobial Peptides: Successes, Challenges and Unanswered Questions. *J. Membr. Biol.* **2011**, *239*, 27−34.
(4) Last, N. B.; Miranker, A. D. Common Mechanism Unites Membrane Poration by Amyloid and Antimicrobial Peptides. *Proc. Natl. Acad. Sci. U. S. A.* **2013**, *110*, 6382−6387.
(5) Chen, J.; Hessler, J. A.; Putchakayala, K.; Panama, B. K.; Khan, D. P.; Hong, S.; Mullen, D. G.; DiMaggio, S. C.; Som, A.; Tew, G. N. Cationic Nanoparticles Induce Nanoscale Disruption in Living Cell Plasma Membranes. *J. Phys. Chem. B* **2009**, *113*, 11179−11185.
(6) Andreu, D.; Ubach, J.; Boman, A.; Wåhlin, B.; Wade, D.; Merrifield, R. B.; Boman, H. G. Shortened Cecropin A-Melittin Hybrids Significant Size Reduction Retains Potent Antibiotic Activity. *FEBS Lett.* **1992**, *296*, 190−194.
(7) Tamang, D. G.; Saier, M. H., Jr. The Cecropin Superfamily of Toxic Peptides. *J. Mol. Microbiol. Biotechnol.* **2006**, *11*, 94−103.
(8) Raghuraman, H.; Chattopadhyay, A. Melittin: A Membrane-Active Peptide with Diverse Functions. *Biosci. Rep.* **2007**, *27*, 189−223.
(9) Schlamadinger, D. E.; Wang, Y.; McCammon, J. A.; Kim, J. E. Spectroscopic and Computational Study of Melittin, Cecropin A, and the Hybrid Peptide CM15. *J. Phys. Chem. B* **2012**, *116*, 10600−10608.
(10) Mancheño, J. M.; Oñaderra, M.; Martínez del Pozo, A.; Díaz-Achirica, P.; Andreu, D.; Rivas, L.; Gavilanes, J. G. Release of Lipid Vesicle Contents by an Antibacterial Cecropin A-Melittin Hybrid Peptide. *Biochemistry* **1996**, *35*, 9892−9899.
(11) Marrink, S. J.; de Vries, A. H.; Tieleman, D. P. Lipids on the Move: Simulations of Membrane Pores, Domains, Stalks and Curves. *Biochim. Biophys. Acta, Biomembr.* **2009**, *1788*, 149−168.
(12) Matyus, E.; Kandt, C.; Tieleman, D. P. Computer Simulation of Antimicrobial Peptides. *Curr. Med. Chem.* **2007**, *14*, 2789−2798.
(13) Herce, H. D.; Garcia, A. E. Molecular Dynamics Simulations Suggest a Mechanism for Translocation of the HIV-1 TAT Peptide across Lipid Membranes. *Proc. Natl. Acad. Sci. U. S. A.* **2007**, *104*, 20805−20810.
(14) Sengupta, D.; Leontiadou, H.; Mark, A. E.; Marrink, S. J. Toroidal Pores Formed by Antimicrobial Peptides Show Significant Disorder. *Biochim. Biophys. Acta, Biomembr.* **2008**, *1778*, 2308−2317.
(15) Leontiadou, H.; Mark, A. E.; Marrink, S. J. Antimicrobial Peptides in Action. *J. Am. Chem. Soc.* **2006**, *128*, 12156−12161.
(16) Herce, H. D.; Garcia, A. E.; Litt, J.; Kane, R. S.; Martin, P.; Enrique, N.; Rebolledo, A.; Milesi, V. Arginine-Rich Peptides Destabilize the Plasma Membrane, Consistent with a Pore Formation Translocation Mechanism of Cell-Penetrating Peptides. *Biophys. J.* **2009**, *97*, 1917−1925.
(17) Neale, C.; Hsu, J. C. Y.; Yip, C. M.; Pomès, R. Indolicidin Binding Induces Thinning of a Lipid Bilayer. *Biophys. J.* **2014**, *106*, L29−L31.
(18) Wang, Y.; Zhao, T.; Wei, D.; Strandberg, E.; Ulrich, A. S.; Ulmschneider, J. P. How Reliable Are Molecular Dynamics Simulations of Membrane Active Antimicrobial Peptides? *Biochim. Biophys. Acta, Biomembr.* **2014**, *1838*, 2280−2288.

DOI: 10.1021/acs.jctc.6b00265
J. Chem. Theory Comput. 2016, 12, 4524−4533

(19) Tieleman, D. P.; Marrink, S. J. Lipids out of Equilibrium: Energetics of Desorption and Pore Mediated Flip-Flop. *J. Am. Chem. Soc.* **2006**, *128*, 12462−12467.
(20) Bennett, W. F. D.; Sapay, N.; Tieleman, D. P. Atomistic Simulations of Pore Formation and Closure in Lipid Bilayers. *Biophys. J.* **2014**, *106*, 210−219.
(21) Sapay, N.; Bennett, W. F. D.; Tieleman, D. P. Thermodynamics of Flip-Flop and Desorption for a Systematic Series of Phosphatidylcholine Lipids. *Soft Matter* **2009**, *5*, 3295.
(22) Bennett, W. F. D.; Sapay, N.; Tieleman, D. P. Atomistic Simulations of Pore Formation and Closure in Lipid Bilayers. *Biophys. J.* **2014**, *106*, 210−219.
(23) Awasthi, N.; Hub, J. S. Simulations of Pore Formation in Lipid Membranes: Reaction Coordinates, Convergence, Hysteresis, and Finite-Size Effects. *J. Chem. Theory Comput.* **2016**, *12*, 3261−3269.
(24) Mirjalili, V.; Feig, M. Density-Biased Sampling: A Robust Computational Method for Studying Pore Formation in Membranes. *J. Chem. Theory Comput.* **2015**, *11*, 343−350.
(25) Shaw, D. E.; Deneroff, M. M.; Dror, R. O.; Kuskin, J. S.; Larson, R. H.; Salmon, J. K.; Young, C.; Batson, B.; Bowers, K. J.; Chao, J. C. Anton, a Special-Purpose Machine for Molecular Dynamics Simulation. *Commun. ACM* **2008**, *51*, 91−97.
(26) Hong, C.; Tieleman, D. P.; Wang, Y. Microsecond Molecular Dynamics Simulations of Lipid Mixing. *Langmuir* **2014**, *30*, 11993−12001.
(27) Phillips, J. C.; Braun, R.; Wang, W.; Gumbart, J.; Tajkhorshid, E.; Villa, E.; Chipot, C.; Skeel, R. D.; Kale, L.; Schulten, K. Scalable Molecular Dynamics with NAMD. *J. Comput. Chem.* **2005**, *26*, 1781−1802.
(28) Lim, J. B.; Rogaski, B.; Klauda, J. B. Update of the Cholesterol Force Field Parameters in CHARMM. *J. Phys. Chem. B* **2012**, *116*, 203−210.
(29) Klauda, J. B.; Venable, R. M.; Freites, J. A.; O'Connor, J. W.; Tobias, D. J.; Mondragon-Ramirez, C.; Vorobyov, I.; MacKerell, A. D., Jr.; Pastor, R. W. Update of the CHARMM All-Atom Additive Force Field for Lipids: Validation on Six Lipid Types. *J. Phys. Chem. B* **2010**, *114*, 7830−7843.
(30) Andersen, H. C. RATTLE: A "Velocity" Version of the SHAKE Algorithm for Molecular Dynamics Calculations. *J. Comput. Phys.* **1983**, *52*, 24−34.
(31) Miyamoto, S.; Kollman, P. A. SETTLE: An Analytical Version of the SHAKE and RATTLE Algorithm for Rigid Water Models. *J. Comput. Chem.* **1992**, *13*, 952−962.
(32) Darden, T.; York, D.; Pedersen, L. Particle Mesh Ewald: An N·Log (N) Method for Ewald Sums in Large Systems. *J. Chem. Phys.* **1993**, *98*, 10089−10092.
(33) Berendsen, H. J. C.; Postma, J. P. M.; van Gunsteren, W. F.; DiNola, A.; Haak, J. R. Molecular Dynamics with Coupling to an External Bath. *J. Chem. Phys.* **1984**, *81*, 3684−3690.
(34) Hess, B.; Kutzner, C.; van der Spoel, D.; Lindahl, E. GROMACS 4: Algorithms for Highly Efficient, Load-Balanced, and Scalable Molecular Simulation. *J. Chem. Theory Comput.* **2008**, *4*, 435−447.
(35) Hess, B.; Bekker, H.; Berendsen, H. J. C.; Fraaije, J. G. E. M. LINCS: A Linear Constraint Solver for Molecular Simulations. *J. Comput. Chem.* **1997**, *18*, 1463−1472.
(36) Essmann, U.; Perera, L.; Berkowitz, M. L.; Darden, T.; Lee, H.; Pedersen, L. G. A Smooth Particle Mesh Ewald Method. *J. Chem. Phys.* **1995**, *103*, 8577−8593.
(37) Berger, O.; Edholm, O.; Jähnig, F. Molecular Dynamics Simulations of a Fluid Bilayer of Dipalmitoylphosphatidylcholine at Full Hydration, Constant Pressure, and Constant Temperature. *Biophys. J.* **1997**, *72*, 2002.
(38) Bussi, G.; Donadio, D.; Parrinello, M. Canonical Sampling through Velocity Rescaling. *J. Chem. Phys.* **2007**, *126*, 014101.
(39) Jämbeck, J. P. M.; Lyubartsev, A. P. Derivation and Systematic Validation of a Refined All-Atom Force Field for Phosphatidylcholine Lipids. *J. Phys. Chem. B* **2012**, *116*, 3164−3179.
(40) Sapay, N.; Bennett, W. F. D.; Tieleman, D. P. Molecular Simulations of Lipid Flip-Flop in the Presence of Model Transmembrane Helices. *Biochemistry* **2010**, *49*, 7665−7673.
(41) Sun, D.; Forsman, J.; Woodward, C. E. Evaluating Force Fields for the Computational Prediction of Ionized Arginine and Lysine Side-Chains Partitioning into Lipid Bilayers and Octanol. *J. Chem. Theory Comput.* **2015**, *11*, 1775−1791.
(42) Epand, R. M.; Vogel, H. J. Diversity of Antimicrobial Peptides and Their Mechanisms of Action. *Biochim. Biophys. Acta, Biomembr.* **1999**, *1462*, 11−28.
(43) Sengupta, D.; Leontiadou, H.; Mark, A. E.; Marrink, S.-J. Toroidal Pores Formed by Antimicrobial Peptides Show Significant Disorder. *Biochim. Biophys. Acta, Biomembr.* **2008**, *1778*, 2308−2317.
(44) Matsuzaki, K.; Yoneyama, S.; Miyajima, K. Pore Formation and Translocation of Melittin. *Biophys. J.* **1997**, *73*, 831.
(45) Cirac, A. D.; Moiset, G.; Mika, J. T.; Kocer, A.; Salvador, P.; Poolman, B.; Marrink, S. J.; Sengupta, D. The Molecular Basis for Antimicrobial Activity of Pore-Forming Cyclic Peptides. *Biophys. J.* **2011**, *100*, 2422−2431.
(46) van Gunsteren, W. F.; Billeter, S. R.; Eising, A. A.; Hünenberger, P. H.; Krüger, P.; Mark, A. E.; Scott, W. R. P.; Tironi, I. G. *Biomolecular Simulation: The {GROMOS96} Manual and User Guide*; Vdf Hochschulverlag AG an der ETH Zürich: Zürich, Switzerland, 1996; pp 1−1042.
(47) Anézo, C.; de Vries, A. H.; Höltje, H.-D.; Tieleman, D. P.; Marrink, S.-J. Methodological Issues in Lipid Bilayer Simulations. *J. Phys. Chem. B* **2003**, *107*, 9424−9433.
(48) Zhao, W.; Róg, T.; Gurtovenko, A. A.; Vattulainen, I.; Karttunen, M. Atomic-Scale Structure and Electrostatics of Anionic Palmitoyloleoylphosphatidylglycerol Lipid Bilayers with Na+ Counterions. *Biophys. J.* **2007**, *92*, 1114−1124.
(49) Sun, D.; Forsman, J.; Woodward, C. E. Atomistic Molecular Simulations Suggest a Kinetic Model for Membrane Translocation by Arginine-Rich Peptides. *J. Phys. Chem. B* **2015**, *119*, 14413−14420.
(50) Li, L. B.; Vorobyov, I.; Allen, T. W. The Role of Membrane Thickness in Charged Protein-Lipid Interactions. *Biochim. Biophys. Acta, Biomembr.* **2012**, *1818*, 135−145.
(51) Wang, Y.; Hu, D.; Wei, D. Transmembrane Permeation Mechanism of Charged Methyl Guanidine. *J. Chem. Theory Comput.* **2014**, *10*, 1717−1726.
(52) Huang, K.; García, A. E. Effects of Truncating van Der Waals Interactions in Lipid Bilayer Simulations. *J. Chem. Phys.* **2014**, *141*, 105101.
(53) van Meer, G.; Voelker, D. R.; Feigenson, G. W. Membrane Lipids: Where They Are and How They Behave. *Nat. Rev. Mol. Cell Biol.* **2008**, *9*, 112−124.
(54) Liu, J.; Conboy, J. C. 1, 2-Diacyl-Phosphatidylcholine Flip-Flop Measured Directly by Sum-Frequency Vibrational Spectroscopy. *Biophys. J.* **2005**, *89*, 2522−2532.
(55) Botan, A.; Favela-Rosales, F.; Fuchs, P. F. J.; Javanainen, M.; Kanduč, M.; Kulig, W.; Lamberg, A.; Loison, C.; Lyubartsev, A.; Miettinen, M. S. Toward Atomistic Resolution Structure of Phosphatidylcholine Headgroup and Glycerol Backbone at Different Ambient Conditions. *J. Phys. Chem. B* **2015**, *119*, 15075−15088.

DOI: 10.1021/acs.jctc.6b00265
J. Chem. Theory Comput. 2016, 12, 4524−4533